Thamires Canuto de Almeida e Silva, Viviane Fernandes Kettermann,
Claudia Pereira , Manuel Simões, Michaela Wilhelm, and Kurosch Rezwan

Novel tape-cast SiOC-based porous ceramic electrode materials for potential application in bioelectrochemical systems

Recommended Citation (primary publication/Version of Record) incl. DOI:

Canuto de Almeida e Silva, T., Fernandes Kettermann, V., Pereira, C. et al. Novel tape-cast SiOC-based porous
ceramic electrode materials for potential application in bioelectrochemical systems. J Mater Sci 54, 6471–6487
(2019). https://doi.org/10.1007/s10853-018-03309-3

Novel tape-cast SiOC-based porous ceramic electrode materials for potential application in bioelectrochemical systems

Thamires Canuto de Almeida e Silva[1] (iD), Viviane Fernandes Kettermann[1] (iD),
Claudia Pereira[2] (iD), Manuel Simões[2] (iD), Michaela Wilhelm[1,*] (iD), and Kurosch Rezwan[1,3] (iD)

[1] University of Bremen, Advanced Ceramics, Am Biologischen Garten 2, IW3, 28359 Bremen, Germany
[2] LEPABE, Department of Chemical Engineering, Faculty of Engineering, University of Porto, Rua Dr. Roberto Frias, s/n,
  4200-465 Porto, Portugal
[3] MAPEX Center for Materials and Processes, University of Bremen, 28359 Bremen, Germany

ABSTRACT

One alternative to improve electrochemical performance and long-term applicability in microbial bioelectrochemical systems (BESs) is the use of porous ceramic electrodes. In this work, electrodes of polymer-derived ceramics based on poly(silsesquioxanes) are synthesized, tailoring the properties by varying pyrolysis temperatures and incorporating conductive phases. Carbon (graphite, carbon black) and metal-based (stainless steel/Cu grids, Co/Ni particles) materials are incorporated into the silicon oxycarbide (SiOC) matrix. The influence of pyrolysis temperature and incorporation of conductive materials on functional properties and electrical conductivity is discussed. Furthermore, this study provides the first investigation of biofilm development on SiOC-based ceramic surfaces with *Escherichia coli* and *Bacillus cereus*. SiOC-based ceramics with DC conductivity values at room temperature in the semiconductor range $(0.044–0.385 \text{ S cm}^{-1})$ were obtained, with the highest values achieved by Co and Ni particles incorporation and in situ formation of CNTs. Adjustment in hydrophilicity and specific surface areas $(6.21–263.45 \text{ m}^2 \text{ g}^{-1})$ is realized by the pyrolysis. The biofilm studies reveal adhesion in the first 2 h for most of the surfaces, with higher bacterial adhesion and biofilm formation with the *E. coli.* The biocompatibility in terms of bacterial attachment and conductivity values comparable to a commercial carbon felt support the applicability of the developed SiOC-based materials as promising new class of electrodes for BES.

Address correspondence to E-mail: mwilhelm@uni-bremen.de

Introduction

The increase in global energy demand and depletion of fossil fuels drive the need of sustainable sources of energy, development of efficient new technologies related to energy conversion and storage with high power and energy densities [1, 2]. Supercapacitors, Li and Na batteries, fuel cells and gas sensors are the main research areas under investigation in fundamental and applied levels [2–6]. Among the new sustainable green technologies, microbial bioelectrochemical systems (BESs) are the prospective area of study in relation to bioenergy production from wastewater treatment [7]. The performance of these devices essentially depends on the properties of their electrode materials; therefore, the development of new electrode materials holds the key to improving these systems [8]. In general, electrode materials vary in properties like electrical conductivity, electrochemical stability, surface areas and electrode/electrolyte contact area, biocompatibility and mechanical strength [7, 8]. Carbon-based materials have been widely applied as electrode materials due to their advantages such as low cost, easy processability, wide potential window, relatively inert electrochemistry, electrocatalytic activity for a variety of redox reductions and nontoxicity [9, 10]. A major drawback of carbon-based materials is still the necessity to control the thermal and electrochemical oxidative degradation under operating conditions [11]. One alternative to improve electrochemical performance and long-term applicability is the use of porous ceramics electrodes. Porous electrodes are used to increase the surface area for charge transfer, thereby reducing the electrode overpotential, as well as to increase the charge storage capacity of capacitive electrochemical systems [1, 12]. Additionally, an optimized porous structure, to accommodate bacteria cells and maintain the access of nutrients through the pores in BES, is desirable [13, 14]. Due to outstanding features, such as high chemical durability, creep resistance, semiconductor behavior, adjusted porosity and surface characteristics, polymer-derived ceramics (PDCs) are a promising class of new materials to address and improve the properties required for electrode materials and provide a porous structure [15, 16]. PDCs represent a class of ceramics which can be synthesized via cross-linking and pyrolysis of suitable polymeric precursors that will consolidate into ceramics upon heat treatment [17]. Silicon oxycarbide (SiOC) is an interesting system of PDCs where properties can be tailored by varying chemical composition and pyrolysis conditions [15]. The tailorable properties in these materials have already attracted interests for electrochemical applications as electrocatalysts [18], as electrode materials in lithium-ion batteries [19–21] and supercapacitors [20]. However, there have been no studies combining adjustment in porosity and surface characteristic, as well as, electrical conductivity and biocompatibility, which would raise possibilities of making them appropriate candidates for new environmentally friendly technologies such as BES.

Most of the studies focus on the improvement in electrical properties in SiOCs ceramics with the use of suitable conductive materials that form percolation paths, thereby decreasing the resistance to electron conduction. On the other hand, the investigation of biocompatibility, in means of bacterial adhesion, of SiOC-based surfaces for engineering applications has not been yet thoroughly considered in the literature. Regarding positive effects of integration of conductive constituents on electrical conductivity, Colombo et al. [22] reported the use of fillers such as $MoSi_2$, α-SiC and graphite in amounts up to 80 wt%, as well as, use of copper acetate (up to 80 wt%) and Cu_2O (up to 30 wt%) in SiOC ceramic foams and obtained values of electrical conductivity from 1.4×10^{-5} to 45.5 Ω^{-1} cm^{-1} at room temperature. By varying ratio of graphite, carbon black and molybdenum disilicide, Drillet et al. obtained conductivity in the range of 0.004–0.305 S cm^{-1} in SiOC-based air cathode [23]. The influence of carbon nanotubes and graphene oxide incorporation into a SiOC matrix was investigated by Moni et al. [24]. An increase in DC conductivity by 3–4 orders of magnitude was found with incorporation of 5 wt% nanofilers (2.97×10^{-9} S cm^{-1}, 2.5×10^{-6} S cm^{-1}–5 wt% GO and 2.1×10^{-5} S cm^{-1}–5 wt% CNT) [24]. In terms of metal-loaded polymer-derived ceramic materials, Scheffler et al. investigated the influence of nickel on the structural evolution of the carbon phase. A decrease in electrical resistivity from 3×10^3 to 0.5 Ω cm was found when the filler-free samples and filler-loaded (1 wt% elemental Ni in the preceramic polymer matrix) pyrolyzed at 1000 °C were compared, respectively. Moreover, the formation of multiwall carbon nanotubes was observed within the pores [25]. Besides electrical conductivity, the surface properties of the

material play a crucial role in current generation. Recent reports based on functional ceramic electrode composite materials of metal oxides with conductive materials in BES endorsed hydrophilicity [26], large surface areas [27] and biocompatibility [27, 28] to the obtained performance improvement.

In this work, porous ceramic materials based on poly(silsesquioxanes) as starting material were synthesized by tape-casting technique, tailoring the properties by varying pyrolysis temperatures and incorporating conductive phases like carbon fillers and metal-based conductive materials. Pyrolysis was conducted under N_2 atmosphere with varying temperatures of 500–1500 °C and six types of conductive materials were incorporated. The influence of pyrolysis temperature and incorporation of conductive materials on morphology, pore size distribution and specific surface area, surface characteristics, electrical conductivity and chemical stability is discussed. Furthermore, biofilm studies are, for the first time, presented with regard to SiOC-based ceramics targeting its potential upcoming application as a BES electrode material. In addition, the functional properties were also compared to carbon felt, a usual electrode applied in BES.

## Experimental section

Materials

As starting materials, commercial poly(methyl silsesquioxane) (Silres® MK, Wacker Chemie AG) and poly(methyl phenyl silsesquioxane) (Silres® H44, Wacker Chemie AG) were used as polymer-to-ceramic precursors. Based on previous works of the research group, graphite (KS75, IMERYL Graphite and Carbon) was added as first carbon-based conductive filler for increment of electrical conductivity and additives such as molybdenum disilicide (MoSi$_2$, abcr GmbH) and azodicarbonamide (Az, azodicarboxamide Sigma-Aldrich Co) were added in means of controlling shrinkage and inducing formation of pores, respectively [23]. In order to further increase electrical conductivity, an additional carbon-based conductive filler, carbon black (CB, Cabot), was used. For the metal-containing electrode materials, metallic grids of copper (Cu, The Mesh Company Ltd) and stainless steel (SS, The Mesh Company Ltd) were integrated during the preparation of the samples. For the same purpose, cobalt and nickel chloride (CoCl$_2$ and NiCl$_2$, Alfa Aesar) were used as a metal source for the formation of metal particles within the PDC matrix. Xylene (Sigma-Aldrich Co) was used as solvent in the preparation and imidazole (Imi, Alfa Aesar) was used as catalyst for the cross-linking process. For comparison purposes, a commercial carbon felt (CGT Carbon GmbH) was used in some of the characterizations.

Electrodes preparation

The electrodes preparation route is depicted in Fig. 1 and starts by dissolving the precursors MK and H44 (in a weight ratio 1:1) in xylene followed by the dispersion of the additives (MoSi$_2$ and Az) and conductive fillers under stirring at room temperature. For the materials with metal particles, the metal salts (CoCl$_2$ and NiCl$_2$) were additionally used in the dispersion step. The amount of solvent was kept as low as possible to achieve a sufficient viscosity for further casting. The cross-linking process starts by adding the catalyst (Imi) into the mixture, which was kept under constant stirring for 20 min. After that, the materials were tape casted using a doctor blade with the gap set at 1.5 and 5 mm. For the materials with metallic grids (Cu and SS), the grids were integrated subsequently after to the tape-casting step. The tapes were then dried at room temperature for 24 h and cut in square shapes with dimensions varying between $10 \times 10 \times 1.5$ mm and $50 \times 50 \times 5$ mm. The cross-linked tapes were pyrolyzed in order to convert the precursors into a hybrid ceramic or a ceramic material. The pyrolysis was performed under an N_2 atmosphere at temperatures between 500 and 1500 °C, with the heating up of 120 K h^{-1} up to 100 °C below the final temperature and 30 K h^{-1} to the final temperature, with a dwelling time of 4 h. A cooling rate of 120 K h^{-1} was applied to end the pyrolysis step. For the metal-containing/integrated electrode materials, only 1000 °C was applied. The obtained SiOC-based materials were denoted with regard to the wt% of the polysiloxane (PS) and conductive materials solid components, in the total mass of the composition and respective pyrolysis temperature used. For the materials with metallic grids, Cu and SS are indicated as the material variety but not considered as wt%. The denotation, composition of the materials and

Figure 1 Processing route, materials and structure of the synthesized electrode materials.
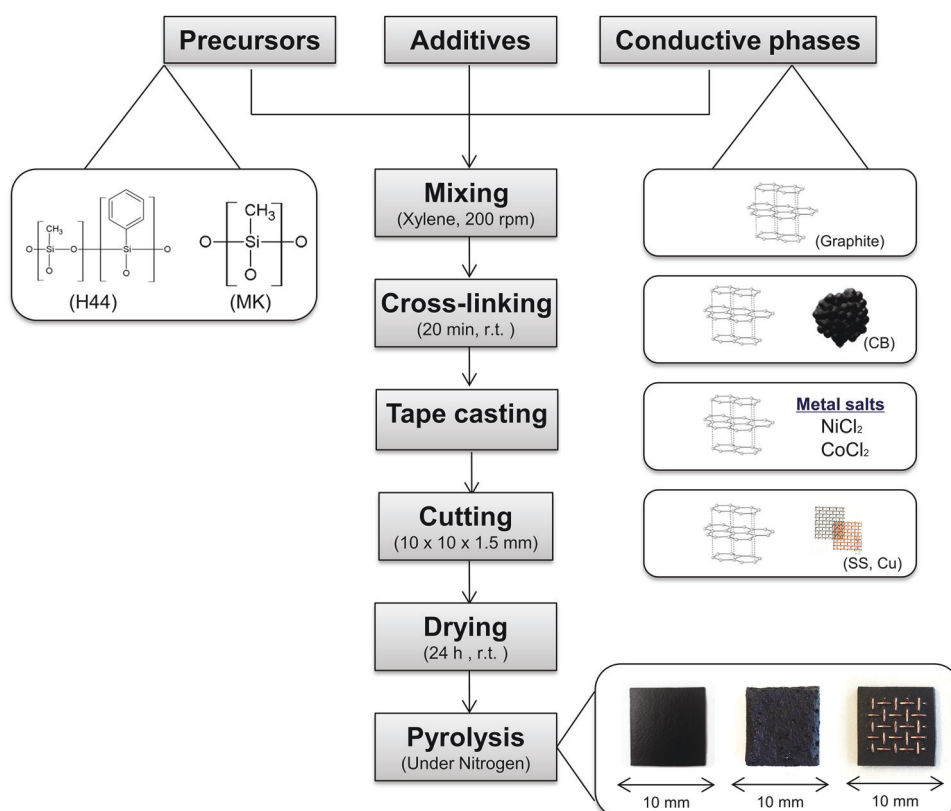
Table 1 Materials composition (wt%) of the cross-linked materials prepared and pyrolysis temperatures applied

Materials denotation (wt%)	H44	MK	$MoSi_2$	KS75	CB	Az	Imi	Metal salt	Pyrolysis temperature (°C)
60PS-600	30.5	30.5	12.0	–	–	26.0	1.0	–	600
60PS-1000	30.5	30.5	12.0	–	–	26.0	1.0	–	1000
42PS-31G-500	21.1	21.1	8.4	30.8	–	17.7	0.9	–	500
42PS-31G-600	21.1	21.1	8.4	30.8	–	17.7	0.9	–	600
42PS-31G-1000	21.1	21.1	8.4	30.8	–	17.7	0.9	–	1000
42PS-31G-1200	21.1	21.1	8.4	30.8	–	17.7	0.9	–	1200
42PS-31G-1500	21.1	21.1	8.4	30.8	–	17.7	0.9	–	1500
40PS-30G-5CB-1000	20.0	20.0	8.0	29.2	5.0	17.0	0.8	–	1000
40PS-30G-5Co-1000	20.0	20.0	8.0	29.2	–	17.0	0.8	5.0	1000
40PS-30G-5Ni-1000	20.0	20.0	8.0	29.2	–	17.0	0.8	5.0	1000
42PS-31G-SS-1000	21.1	21.1	8.4	30.8	–	17.7	0.9	–	1000
42PS-31G-Cu-1000	21.1	21.1	8.4	30.8	–	17.7	0.9	–	1000

pyrolysis temperature applied are described in Table 1.

Materials characterization

Scanning electron microscopy (SEM, Supra 40-Carl Zeiss, Germany) was used in order to investigate the morphology and structural changes of the material after pyrolytic conversion. Formation of metal particles was observed by transition electron microscopy (TEM-EM 900, Carl Zeiss, Germany). Micro–meso-porosities and BET (Brunauer, Emmett and Teller)-specific surface areas (SSA) were determined by nitrogen adsorption isotherms measured at 77 K using Belsorp-mini (Bel Japan, Inc.) device. The materials were pretreated at 120 °C for 3 h under

vacuum. For determination of meso–macroporosities and pore size distribution, mercury intrusion porosimetry (Pascal 140/440, POROTECH GmbH) was applied. The surface characteristics were analyzed by adsorption of n-heptane and water. For this, 0.5 g of sample (particle size $\leq$ 300 μm) was stored into vessels and inside closed Erlenmeyer flasks filled with water or n-heptane at room temperature and at equilibrium with its vapor phase. After 24 h, the materials in the adsorptive atmosphere were weighed again to determine the vapor uptake [29]. With the values of BET-specific surface area acquired, the uptake was recalculated into g m^{-2}. The surface wettability was assessed by water contact angle measurements, carried out on a pendant drop tensiometer (OCA25, DataPhysics, Germany). The surfaces were polished, cleaned and dried prior the analysis. The electrical conductivity measurements were carried out using the impedance analyzer (Impedance Measurement Unit IM6ex Zahner Electric) connected with the software THALES, in the frequency range of 1 MHZ to 10 mHZ with AC amplitude of 10 mV at 25 °C [24]. The chemical stability was analyzed by the change of the dry weight of the materials placed in 30 ml of phosphate buffer solution (PBS, pH 7), at room temperature over a period of 4 weeks. The materials were previously placed in an oven at 70 °C for 6 h, cooled and weighed. Every seventh day, the materials were then rinsed with distilled water, dried, weighed and immersed again in PBS solution.

Bacterial culture conditions and biofilm assays

As model microorganism, a gram-negative bacterium *Escherichia coli* (CECT 434) and a gram-positive bacterium *Bacillus cereus* (a strain isolated from a biocide solution [30]) were used for the adhesion and biofilm experiments. The bacteria were chosen due to its biofilm forming ability [31, 32] likewise its applicability in BES [26, 27, 33]. The bacterial suspensions were grown overnight in Mueller–Hinton broth (MHB, Merck, VWR) at 30 °C and 120 rpm. The cells were centrifuged (3999 g, 15 min, 25 °C) and washed with saline solution. The concentration of the bacterial solution was adjusted to a final concentration of 1×10^8 colony forming units (CFU)/ml. Electrode materials with dimensions of $1 \times 1 \times 0.1$ cm, after sterilization by UV exposure for 20 min (each

surface), were immersed in 1 ml of bacterial solution and incubated for 2 h (adhesion) and 24 h (biofilm formation) at 30 °C under constant stirring (120 rpm) in a 48-well microtiter plate (Corning), according to Malheiro et al. [34]. To evaluate the cell viability, after the defined periods the materials were vortexed in 5 ml (adhesion) and 9 ml (biofilm formation) of saline solution (0.85% NaCl) for 1 min to provide the detachment of the cells. After dilution, the detached cells were assessed in terms of CFU in Mueller–Hinton agar after 24 h of incubation at 30 °C. The counts were normalized to the exposed area of the material tested and expressed in CFU per cm^{-2}. Three independent experiments with replicates were performed for each bacterium/material.

Statistical analysis

Bacterial adhesion and biofilm formation data were analyzed using GraphPad Prism 7. The mean and standard deviation within samples were calculated in all cases. Because low sample numbers contributed to uneven variation, the nonparametric Kruskal–Wallis test was used. Statistical calculations were based on confidence level equal or higher than 95% (P > 0.05 was considered statistically significant).

Results and discussion

Macrostructure characterization

SiOC-based electrodes materials were produced by tape-casting technique with dimensions varying from $10 \times 10 \times 1.5$ mm and scaled-up till $50 \times 50 \times 5$ mm. The green tapes were stable and easy to cut. The pyrolyzed tapes presented the so-called black glass look and appropriate handling stability. In this work, ca. 17 wt% azodicarboxiamide was used as a foaming agent to induce the formation of pores [23]. Additionally, the pore sizes could be adjusted by applying different pyrolysis temperatures. The foaming agent decomposes around 200 °C and leaves cavities behind in the matrix producing porous materials. With regard to compensating the shrinkage and weight loss of the tapes during the ceramic conversion of polymers, ca. 8 wt% MoSi$_2$ was used as filler based in the optimized amount of previous studies [23]. The resulting macrostructure was investigated by SEM, and the pyrolyzed electrode

materials are shown in Fig. 2. Figure 2a illustrates the graphite-containing material pyrolyzed at 500 °C, which presents smaller pores due to an incomplete polymer-to-ceramic conversion. This incomplete conversion results in hybrid materials with pronounced microporosity [35], which is why a similar structure is observed for the material pyrolyzed at 600 °C. Above 600 °C, amorphous ceramics are obtained, the microporosity collapses, and the macropore formation is pronounced providing chemical and mechanical stability [15, 36]. Figure 2b shows the graphite-containing material pyrolyzed at 1000 °C where bigger pores can be observed. Similar structure was found for the material pyrolyzed at 1200 °C. In general, the SEM analysis revealed pores sizes in the range of 0.5–40 μm for all pyrolyzed electrode materials. When the pyrolysis is carried out above 1400 °C and under N_2 atmosphere, different phases like SiC-Si_3N_4-Si_2N_2O can be built [37]. Figure 2c shows the graphite-containing material pyrolyzed at 1500 °C for which a structural change and the formation of Si_3N_4 whiskers (left side) were found.

In metallic grid-containing materials, SS and Cu grids were integrated on the surface of the PDC matrix after the tape-casting step. Figure 2d shows the SS grid-integrated graphite-containing material with a grid aperture of 1.20 mm and a wire diameter of 0.4 mm. A few cracks were observed in the matrix which is the result of different thermal expansion coefficients of metal grids and ceramic matrix. A similar behavior was observed for the Cu grid-integrated material. In general, the introduction of metal particles influences pyrolytic conversion, stabilization of phases, as well as material properties [38]. For the metal-containing materials, metal salts were used as sources of Co and Ni particles. By metal ions reduction during pyrolysis, metal nanoparticles could be generated within the SiOC matrix [25]. The metal content after pyrolysis at 1000 °C was

Figure 2 SEM images of the pyrolyzed electrode materials at 500, 1000, 1500 °C (**a**, **b**, **c**), materials integrated with SS grids (**d**) and Co/Ni-containing materials (**e**, **f**).
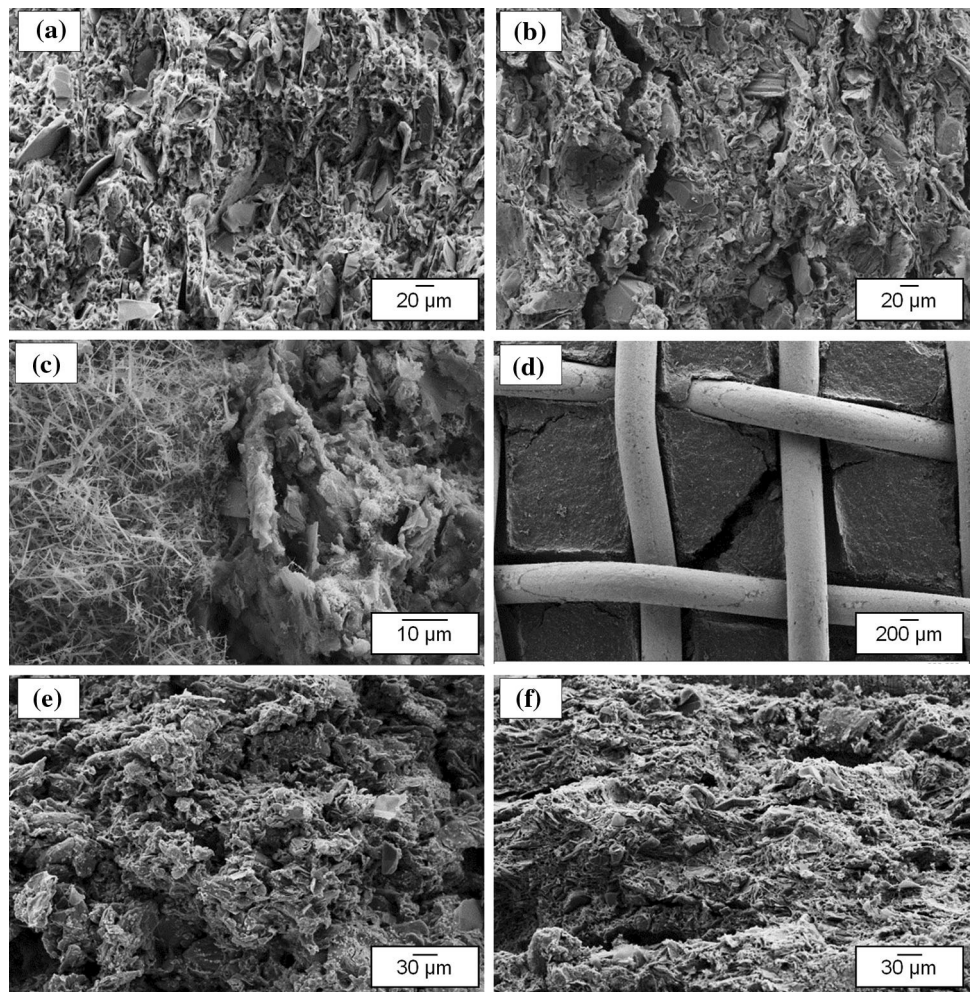
calculated on the basis of thermogravimetric measurements (Fig. S1), resulting in an amount of 2.88 and 1.69 wt% for Co- and Ni-containing materials, respectively. In Fig. 2e, f, the morphology of Co and Ni-graphite-containing materials are shown. The Co/Ni-containing materials show a rough surface and a pore arrangement which differs from the metal-free material pyrolyzed at 1000 °C (Fig. 2b) confirming the influence of metal presence on the near net shape of the material. Bacteria sizes can range from 200 nm to 750 μm [39], though in BES their sizes are typically 0.5–5.0 μm in length. The resulting structure of all the synthesized materials provides a suitable size for accommodating bacteria as well as the feasibility of nutrients access through the pores and internal colonization.

Pore size distribution and specific surface area

Pore size and their distribution are important parameters that influence physical properties of porous materials and also determine reaction/active sites in electrochemical applications. In order to characterize the micro–meso–macroporosity of the materials synthesized, nitrogen adsorption/desorption isotherms were recorded and mercury intrusion porosimetry was applied. The isotherms and corresponding SSAs are shown in Fig. 3.
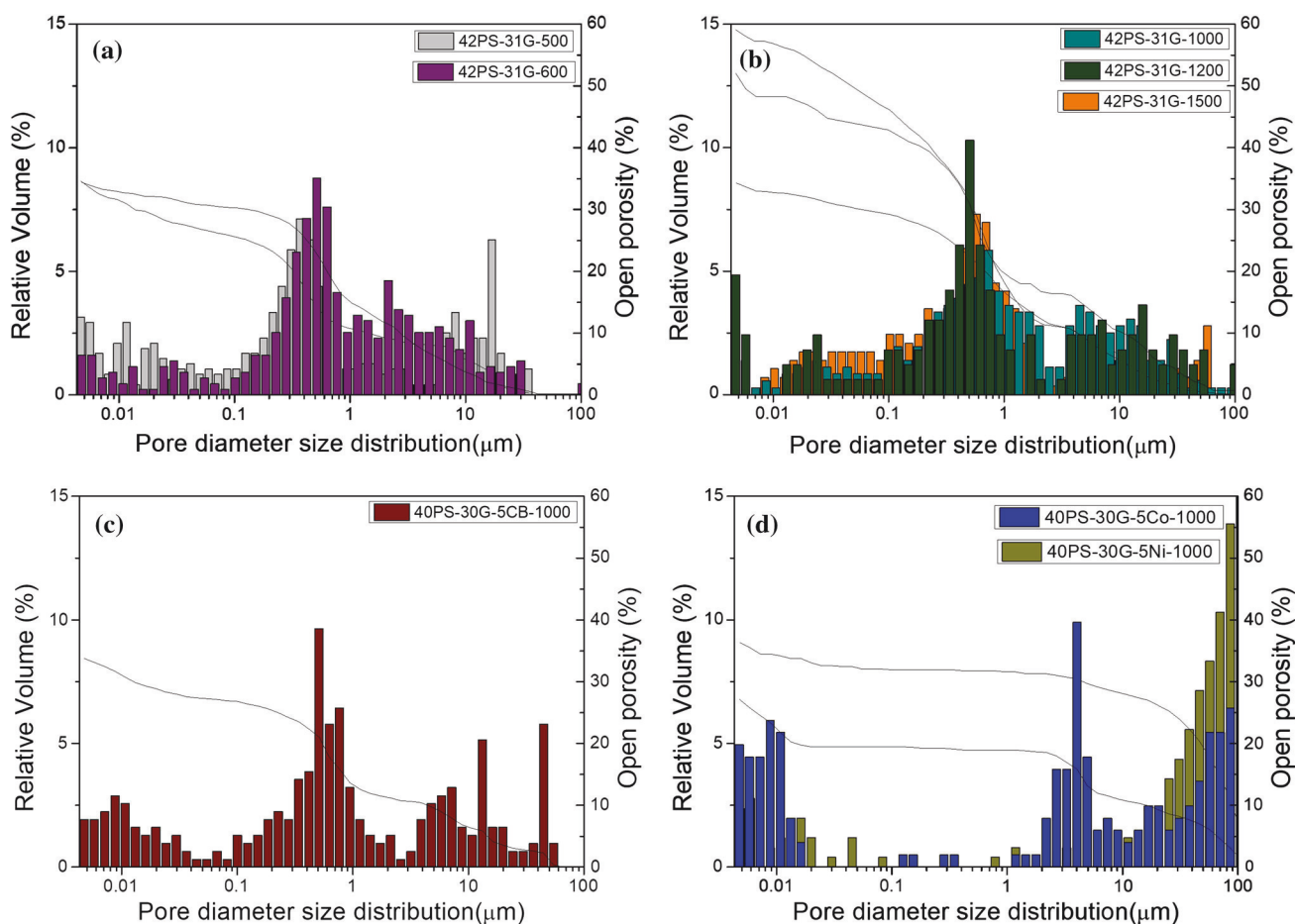
For the electrode materials pyrolyzed at 500 and 600 °C, the isotherms are classified as type I [40] which characterizes micropores (pore
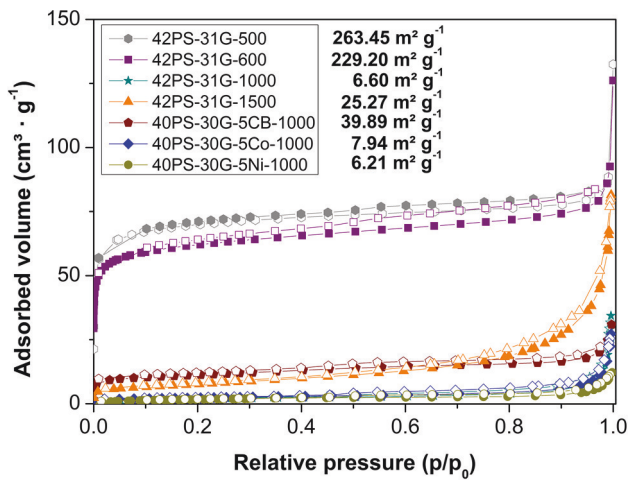
diameter < 2 nm) [41] filled at low relative pressures. These micropores are generated during the partial polymer-to-ceramic conversion upon pyrolysis between 400 and 800 °C [42–44], as transient porosity and resulting in higher specific surface areas (230–265 m^2 g^{-1}). For the materials pyrolyzed at 1000 °C, type IV isotherms [40] (Fig. S2) were observed, which are typical for mesoporous materials (pore diameter 2–50 nm) [41], and show an increase in volume adsorbed at higher relative pressures as well as a hysteresis loop. With increasing pyrolysis temperature, SSAs decrease which is related to the collapse of micropores [44]. As a result, the materials pyrolyzed above 600 °C present lower SSAs of 6–40 m^2 g^{-1}. The isotherm of the material pyrolyzed at 1200 °C was also classified as type IV (Fig. S3). For the material pyrolyzed at 1500 °C, type II isotherm (Fig. S3) was observed, which is correlated to macroporous (pore diameter > 50 nm) [41] or non-porous materials. At this temperature, an increase in specific surface area up to 25 m^2 g^{-1} was observed which can be referred to small gaseous molecules released and simultaneous generation of pores during carbothermal reduction process [45]. Since the graphite (KS75) used in this work has a low SSA of 7 m^2 g^{-1}, the porosity was mainly influenced by the pyrolytic conversion of the silsesquioxanes into ceramics. For the carbon black-containing material, an increase in surface area was observed which is related to the microporosity of the carbon-based filler which possesses an SSA of 44.80 m^2 g^{-1}. For the Co/Ni-containing materials, the type IV isotherms were also observed (Fig. 3, Fig. S2), as for the graphite-containing material pyrolyzed at 1000 °C and SSAs were not significantly affected by the formation and presence of metal particles. As expected, the SSAs of graphite-containing materials without and with grids (SS/Cu) pyrolyzed at 1000 °C are similar. This can be attributed to the integration of the grids which do not influence the micro–mesoporosity of the SiOC matrix. The SSAs of the SiOC-based electrode materials (6.21–263.45 m^2 g^{-1}) are relatively higher compared to a carbon felt characterized in this work (0.032 m^2 g^{-1}) and thus can impact the BES performance by enhancing electrode kinetics. Moreover, the Co/Ni-containing materials could offer reactive sites influencing the electrocatalytic activity toward the oxygen reduction reaction (ORR) that takes place at cathode electrodes in BES.

Figure 3 Nitrogen adsorption–desorption isotherms and SSA of pyrolyzed electrode materials with carbon-based conductive fillers and metal particles.

Figure 4 Relative pore volume, pore size distribution and open porosity of pyrolyzed electrode materials with carbon-based conductive fillers (**a**–**c**) and metal particles (**d**).

Figure 4 shows mercury intrusion results performed for graphite-containing materials pyrolyzed at different temperatures and graphite-carbon black- as well as Co/Ni-containing materials pyrolyzed at 1000 °C. The material pyrolyzed at 500 °C possesses a broad distribution with the main diameters around 0.1 and 1 μm. For the material pyrolyzed at 600 °C, a bimodal distribution and a decrease in relative volume of mesopores was observed. At 1000 °C, an even broader distribution was found, and an increase in relative volume of macropores was observed. The pronounced macroporosity results from the collapse of pores due to the increase in pyrolysis temperature applied. The total porosity of materials pyrolyzed in the range of 500–1000 °C was not significantly affected by the temperature and remains around 34%. For the materials pyrolyzed at 1200 °C and 1500 °C, a similar trend of bimodal distribution and a comparatively narrow region of main diameter between 0.1

and 1 μm were observed. However, the total porosity of 52.02 and 59.09% was increased, compared to the materials pyrolyzed at 1000 °C and below. The change in porosity is due to the phase separation process of SiOC and further carbothermal reduction in silica with free carbon that occurs at higher pyrolysis temperatures (> 1200 °C). At these temperatures, nanocrystallites of SiC and Si_3N_4 are produced with the evolution of gaseous species (i.e., SiO, CO and CO_2) [37, 46, 47].

Concerning the graphite-carbon black-containing material, a trimodal distribution was observed with an increase in the relative volume of mesopores. The open porosity was not influenced by the incorporation of this carbon-based filler. For the Co/Ni-containing materials, the formation of Co and Ni particles led to a shift of the pores in the macropore region with diameters larger than 1 μm. An increase in the relative volume of mesopores compared to the

graphite-containing material pyrolyzed at 1000 °C (metal-free) was also observed. Based on thermogravimetric measurements (Fig. S1), Ni and Co particles catalyze the decomposition process during the pyrolytic conversion and, hence, influence the pore size distribution.

Overall, the synthesized materials pyrolyzed at temperatures up to 600 °C show micro-/mesoporous structures, while materials pyrolyzed at higher temperatures show meso-/macropores. Due to the tailorable porosity achieved, the electrode materials developed can play different roles in providing an optimized porous structure to accommodate bacteria cells as anode electrodes. From the cathode side perspective, the open pores developed can influence in the oxygen transport to the catalyst for the ORR.
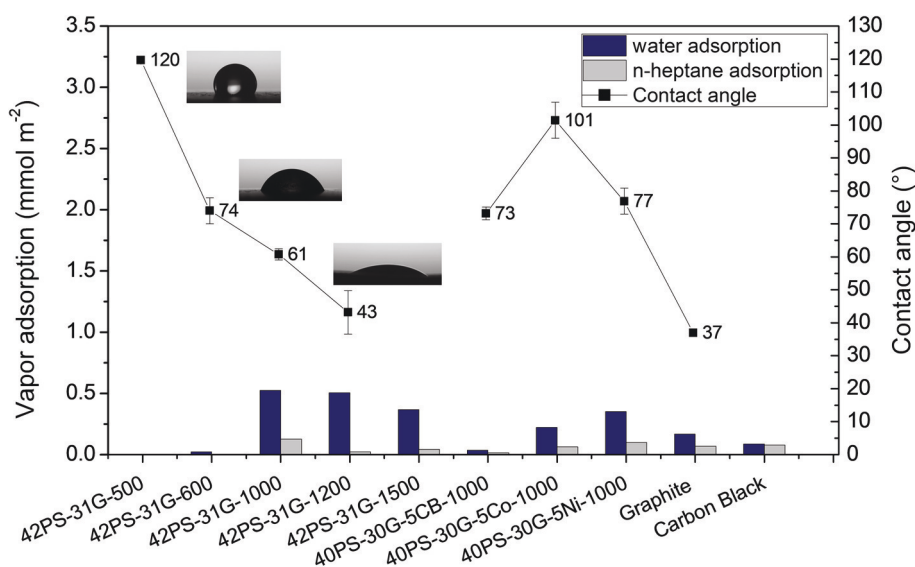
Adjustment of surface characteristics

Surface characteristics are a determining parameter on material–surface interactions regarding adsorption or adhesion in chemical separation processes and coatings [48–50]. Adsorption capacities of solvent vapors of different polarity, polar (water) and non-polar (n-heptane), were investigated in the interest of determining the hydrophilicity and hydrophobicity of the materials synthesized. The materials were compared with regard to ratios of water to n-heptane vapor adsorption. A ratio higher than 1 indicates a higher affinity for water and hence a hydrophilic behavior. The uptakes were related to SSA values and are presented in Fig. 5, and the adsorption ratio is additionally presented in Fig. S4a. The surface wettability was also investigated, and the water contact angle values are displayed in Fig. 5 (right y-axis) and Fig. S4b.

Overall, the materials adsorbed more water vapor than n-heptane, indicating a higher affinity to polar vapors and by that demonstrating a hydrophilic behavior of the surface. The hydrophilicity (the ratio of water/n-heptane vapor adsorbed) greatly increased with the increase in pyrolysis temperature which can be explained by the decomposition of the methyl and phenyl moieties during the pyrolytic conversion of MK and H44 and the evolution of porosity [16]. A pronounced increase in hydrophilicity was seen for the pyrolyzed material at 1200 °C. This increase can be referred to the consumption of free carbon due to the start of carbothermal reduction at this temperature. For the graphite-containing material pyrolyzed at 1500 °C, the decrease in hydrophilicity is correlated with the formation of Si_3N_4. Besides, due to increased open porosity (59.09%), the contact angle measurement of this material could not be performed, because the water was soaked in. Regarding the graphite-carbon black-containing material, a decrease in hydrophilicity was observed, when compared to the graphite-containing material pyrolyzed at 1000 °C, which is connected to the hydrophobic nature of carbon black. Therefore, the increase in total carbon content in the material together with a decrease in hydrophilic silica content led to the decrease in hydrophilicity.

Figure 5 Water and n-heptane max. vapor adsorption related to SSA (columns) and contact angle (black markers) of the pyrolyzed electrodes containing graphite, carbon black and Co/Ni particles and single carbon fillers.

For Co/Ni-containing materials, a slight reduction in hydrophilicity was found. As surface characteristics for the materials integrated with grids (SS/Cu), the value was considered the same as the graphite-containing materials pyrolyzed at 1000 °C. The additional contact angle measurements of water droplets show the gradual increase in wettability with increasing pyrolysis temperature by the decrease in the contact angle values. For the graphite-carbon black- and Ni-containing materials, a hydrophilic behavior was also confirmed by the contact angle (73.2° and 76.9°), whereas for the Co-containing material hydrophobicity (101.4°) was observed. The disagreement to the vapor adsorption results is still under investigation.

In the final result, the surface characteristics of the synthesized materials could be mainly tailored by the pyrolysis temperature applied, making them suitable for different applications that require hydrophilic materials. Regarding bioelectrochemical applications, the tailorability of hydrophilicity of the materials developed can improve surface interactions to enable the growth of anodic electroactive biofilms in BES [51, 52]. In terms of cathode configurations in BES, aqueous-based cathode with dissolved oxygen in the electrolyte and air-based cathode with direct air diffusion are usually applied [53]. A balanced three-phase boundary (liquid, air and solid) is required to provide oxygen transfer, protons migration and flow of electrons maintaining the performance. In order to minimize water filling in the pores in air cathodes, hydrophobic materials are preferable, thus preventing flooding [54]. Therefore, in this context, the choice is limited to the materials developed which presented lower degree of hydrophilicity.

Electrical conductivity

By electrical impedance spectroscopy (EIS) method, the electrical conductivity [$\sigma_{AC}(\omega)$] values of the SiOC-based electrode materials were determined using the equation (Eq. 1).

$$\sigma_{AC}(\omega) = (L/A)x(1/R) \tag{1}$$

where L and A represent the thickness and the cross-sectional area of the material, respectively, and R is the impedance measured. The direct current (DC) conductivity was calculated from conductance spectrums and according to Jonscher's power-law

behavior [55], which describes the frequency dependence to alternating current (AC) conductivity by the following equation (Eq. 2).

$$\sigma_{AC}(\omega) = \sigma_{DC} + A\omega^n \tag{2}$$

where σ_{DC} and σ_{AC} are the DC and AC conductivities of the materials, respectively, A is a pre-exponential constant, ω is the angular frequency and n is the frequency exponent, with $0 < n < 1$. The DC conductivity values of the electrode material measured at room temperature are shown in Fig. 6a in comparison with a commercial carbon felt. Values of DC conductivity of two materials prepared without any incorporation of conductive materials and pyrolyzed
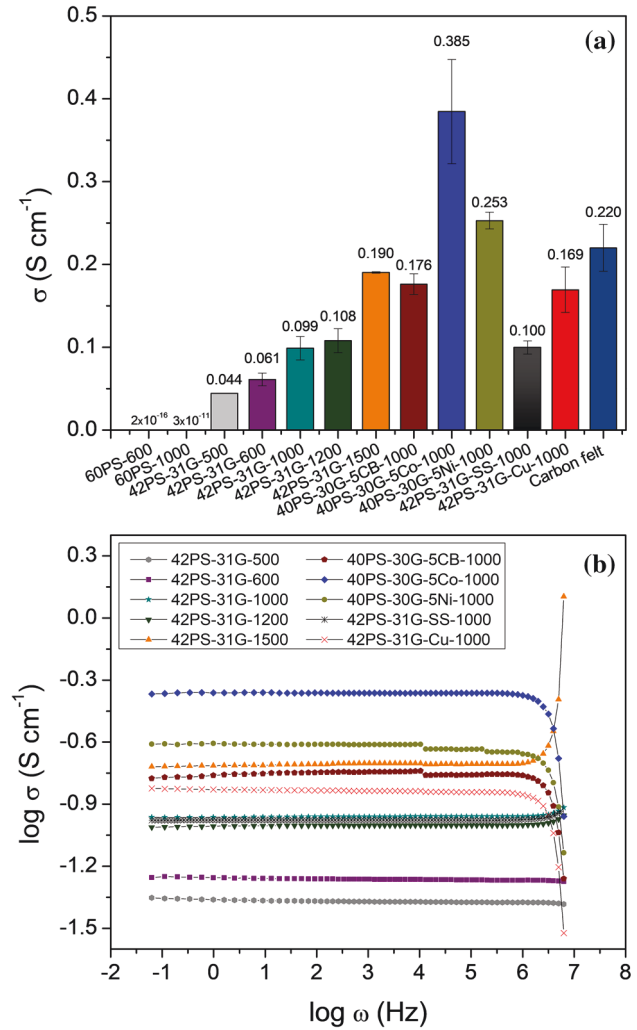
Figure 6 Electrical conductivity values obtained by impedance analyzer (a) and conductance spectra at room temperature of the electrode materials prepared (b).

at 600 and 1000 °C are additionally displayed in Fig. 6a.

The comparison of SiOC-materials free of conductive phases with graphite-containing ones pyrolyzed at 600 and 1000 °C shows an increase in DC conductivity by ∼ 14 and 10 orders of magnitude, respectively. The materials without conductive phases behave like an insulator. The conduction mechanism in SiOC was found to be based on the intrinsic conductivity of turbostratic carbon (formation above 800 °C) [56]. For the materials without incorporated conductive phases, the conduction is based on the bandgap of turbostratic carbon, which gives very low conductivity values [57]. The lack of conduction of the materials in this work was, in a first step, overcome by the use of graphite powder based on loads used in [23] and by changes of the pyrolysis temperature. Comparing the graphite-containing materials pyrolyzed at 500 and 1500 °C (0.044 S cm^{-1} and 0.190 S cm^{-1}), the conductivity values increase by ∼ 1 order of magnitude. Here, since the composition of the materials was kept identical, the electrical conductivity of the SiOC-derived materials is mainly dominated by pyrolysis temperatures applied during the polymer–ceramic conversion. In the temperature range between 700 and 1400 °C, an excess of carbon precipitates forming an interpercolating network that results in a transition from an insulator to a semiconductor [56, 58]. Regarding the combination of graphite and addition of carbon black, an increase of ∼ 1.8-fold in DC conductivity was found. The enhanced conductivity is related to the higher amount of carbon due to its incorporation.

For the materials with integrated metallic grids, an increase of ∼ 1.7-fold in conductivity was found for the Cu-integrated material when compared to the graphite-containing material pyrolyzed at 1000 °C which is due to the low electron resistivity of the metal (Cu). In contrast to Cu-integrated material, SS-integrated material did not show a significant improvement in electrical conductivity without degrading the conductivity compared to the materials without the grid. This can be explained by the fact that stainless steel alloys do not form a crystal lattice where the outer shell electrons are shared and easily move through the lattice (as in copper, silver and gold) and by that, the resistance of electron flow is increased compared to Cu-based materials. The best improvement in electron conductivity could be achieved by incorporation of Co and Ni particles.

Comparing with the DC conductivity of graphite-containing material (0.099 S cm^{-1}), an increase up to fourfold (0.253 S cm^{-1} for Ni and 0.385 S cm^{-1} for Co) was obtained with a metal content of less than 2–3 wt%, as calculated by thermogravimetric analysis. Within the pore structure of the Co/Ni-containing materials, carbon nanotube (CNT) formation could be identified by SEM and TEM analysis, as shown in Fig. 7 for Co-containing material. Metal particles were found either fixed to the matrix and/or also along the length of the tubes formed. The known mechanism of CNT formation describes pores as catalytic microreactors while CNTs emanate from individual metal particles on the ceramic material [25, 56]. The in situ formation of CNTs can also be addressed to the further enhancement of DC conductivity due to the high conductivity of this carbon species.

The DC conductivity of a carbon felt usually used as a commercial electrode material in BES was also measured for comparison reasons. The DC conductivity values of most of the materials are substantially close to the carbon felt value measured (0.22 S cm^{-1}), and for the Co/Ni-containing materials, even higher conductivity values were observed. The sufficient electrical conductivity demonstrated supports the applicability of the new electrode materials in the area of BES.

Even though the electron transfer mechanisms discussed in BES are related to the microorganisms, in order to understand the transport behavior of these materials, frequency dependence studies of AC conductivity were performed. Figure 7a shows the frequency dependences of conductivity measured at 25 °C for the prepared materials, and the individual plots are additionally presented in Fig. S5 and Fig. S6. Regarding the graphite-containing electrode materials pyrolyzed at temperatures from 500 °C to 1500 °C, two main behaviors were observed. From the conductance spectrum of the materials pyrolyzed at 500 and 600 °C (Fig. S5), a conductivity–frequency dependence is shown, where σ decreases with the increase in frequency. The conductivity dependence of frequency can be associated to the low carbon content and low percolation network degree of SiOC-based materials at these pyrolysis temperatures. For the graphite-containing materials pyrolyzed at 1000, 1200 and 1500 °C, a similar tendency was observed. Through the conductance spectrum shown in Fig. S5, a slight increase of σ is observed at lower frequency
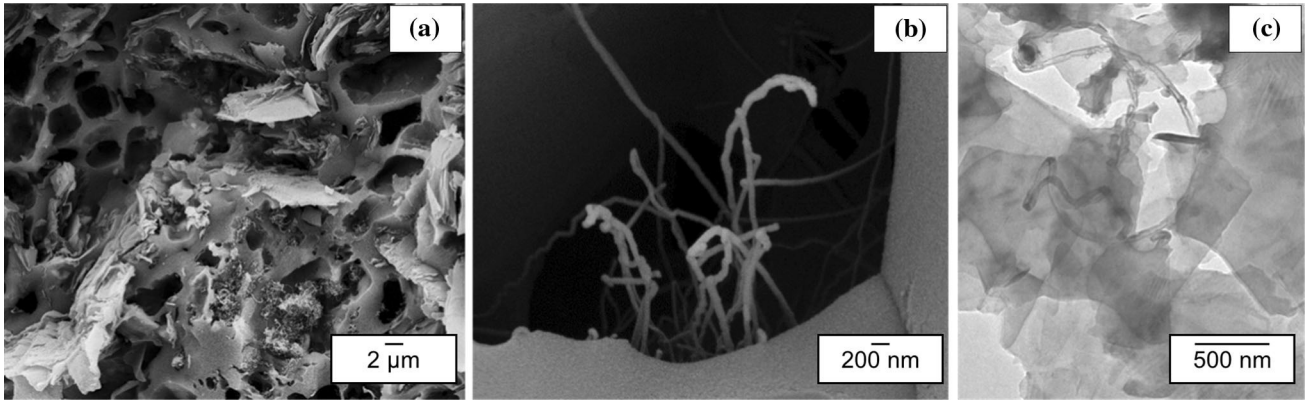
Figure 7 SEM (**a**, **b**) and TEM (**c**) images confirming the carbon nanotubes formation in the Co-containing electrode material prepared.

range, followed by a frequency-independent behavior in the mid-ranges and frequency dispersion at higher frequency range [59]. The independence of frequency at lower mid-frequencies is related to the corresponding DC conductivity of the material and the dispersion at higher frequencies suggesting a hopping conduction mechanism for these materials [59, 60]. For the metallic grids/metal-containing materials, as well as, the carbon black-incorporated material, two distinct behaviors were found and are displayed at Fig. S5 and Fig. S6. The SS-integrated electrode material follows the trend of the materials pyrolyzed at 1000–1500 °C, indicating hopping mechanism. The Cu-integrated, Co/Ni- and the graphite-carbon black-containing materials possess frequency-independent behavior in the lower range of frequency whereas at higher frequency conductivities decreases monotonically with frequency. The decrease of σ_{AC} at higher frequencies is related to the change of conduction mechanism from hopping to metal-like conduction, as well as, enhancement of the skin effect (electric current flow through the "skin" of the conductor) [61, 62].

Chemical stability

With regard to a first impression about the stability of the materials synthesized, neutral conditions and a period of four weeks were chosen as parameters based on the BES environment. The variation of the weight of the dry materials over the period is shown in Fig. 8.

In summary, the materials presented a weight loss/increase lower than 5%, except for the Co-containing material which showed a weight loss of ∼ 10%. With the increase in pyrolysis temperature
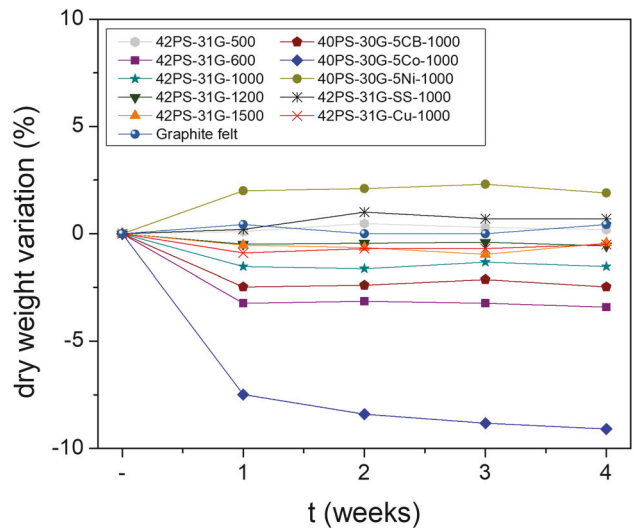
Figure 8 Chemical stability tests in phosphate buffer solution (pH 7) over a period of 4 weeks.

applied (600–1500 °C), a decrease in weight loss is observed. This trend can be associated with the partial decomposition and elimination of organic moieties from the preceramic precursors during pyrolysis, which starts at 400 °C and is not complete until 600 °C [15, 35]. Due to the higher degree of organic load of the polymeric precursors at temperatures below 700 °C, the susceptibility of the materials toward disintegration is higher. Pyrolysis above 800 °C consolidates the amorphous structure of the SiOC-materials, and beyond 1000 °C, the transition to the crystalline phase, followed by phase separation, starts [15]. As a result of the rearrangement of the structure during the heat treatment, the stability is enhanced what is in agreement with the results obtained. The increase in weight loss for the graphite-carbon black-containing material compared to the

graphite-containing pyrolyzed at 1000 °C can be correlated to the higher amount of carbon. This makes the material more susceptible to chemical reactions. The increase in weight, more pronounced for the Ni-containing material, can be accounted to the formation of passive layer (oxide) on the surface exposed. The pronounced increase in weight loss for the Co-containing material can be associated to the change in the built of the structure, affected by the metal incorporation, resulting in larger pores and higher accessibility of the liquid media to allow disintegration. Additionally, leaching of intermediate products formed from thermal decomposition of $CoCl_2$ can be addressed to the higher weight loss.
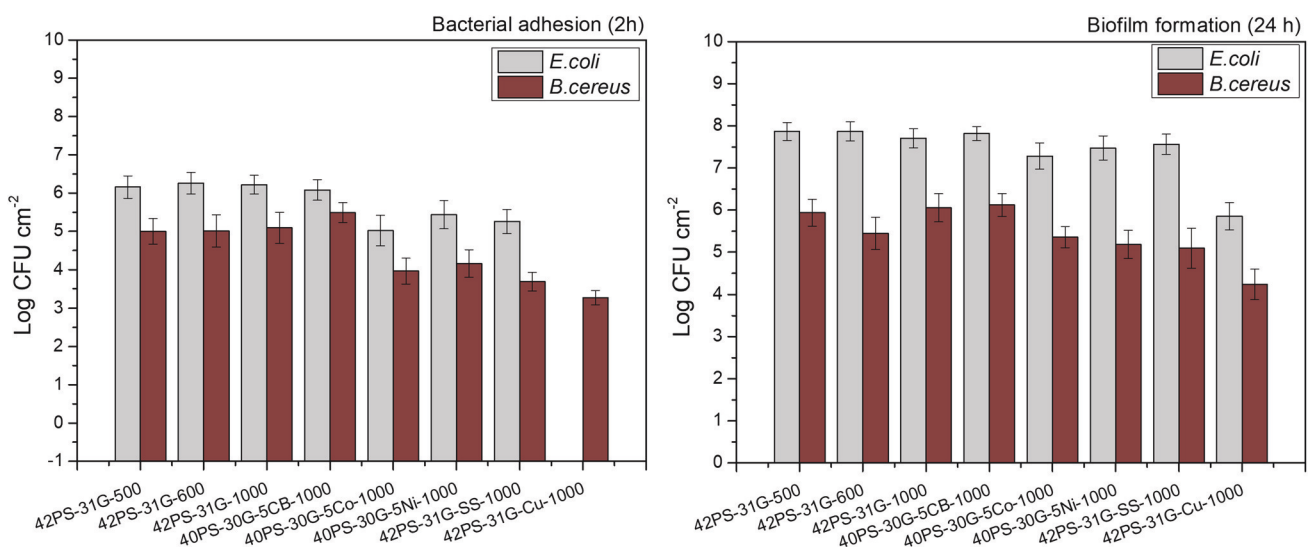
Bacterial adhesion and biofilm formation

The development of a biofilm is a complex multi-step process which leads to the formation of a microbial community adhered to the surface [63]. Biofilms play an important role in nature and recently also in bioelectrochemical technology. *B. cereus* and *E. coli* were used as model bacteria to assess adhesion (2 h) and biofilm formation (24 h) on the SiOC-based surfaces (Fig. 9). It was possible to observe that most of the surfaces allowed adhesion in the first 2 h, except for the Cu grid-containing material using *E. coli*. The number of cells further increases with the 24-h incubation time ($P < 0.05$). Therefore, biofilm formation was observed for all materials. In addition, the

surfaces show higher bacterial adhesion and biofilm formation with *E. coli*.

With regard to the physicochemical properties of the materials obtained by distinct pyrolysis temperature applied (500, 600 and 1000), this seems to have a negligible impact on bacterial adhesion and biofilm formation ($P > 0.05$). Regarding the additional conductive materials, a decrease was observed for metal-based materials, with pronounced reduction for the Cu grid-containing material with both microorganisms ($P < 0.05$). Previous studies reported the use of Ni and Co nanoparticles to prevent bacterial attachment [64, 65]. In this work, a slight reduction is also observed for the Co/Ni-containing materials even though the metal content incorporated is low and not all the particles are exposed on the surface. For the SS/Cu grid-containing materials similarly to Sharifahmadian et al., the bacterial viability was reduced on Cu surfaces while SS did not present antibacterial properties [66]. Nevertheless, the antibacterial activity of cooper is known [67] and low bacterial adhesion was already expected. Although metal electrodes have been considered in BES research, stability concerns during the operation such as passivating oxide layer formation, oxidative dissolution and metal ions released upon oxidation still limit the operative potential window [68]. Adverse effects on biofilm formation due to copper corrosion and toxicity have also been described by Zhu and Logan [69].

In this study, pure cultures of distinct gram-positive and gram-negative microorganisms were used.

Figure 9 *B. cereus* and *E. coli* adhesion (2 h) and biofilm formation (24 h) on the SiOC-based electrode materials. The error bars represent the standard deviations from three independent experiments.

Although the BES operates with these two gram types, mixed culture is the reality in wastewater treatments. Besides, factors such as pH, temperature, shear stress and wastewater composition were not considered in this initial assessment. Therefore, further studies using mixed culture bacteria and considering some of these factors may provide a fine-tuning in the manufacture of SiOC-based electrode materials for BES.

Conclusions

SiOC-based electrodes were synthesized based on poly(silsesquioxanes) containing carbon- and metal-based conductive materials and assessed in terms of porosity, surface characteristics, electrical properties and bacterial attachment. The electrical conductivity of SiOC-materials increases by ~ 1 order of magnitude with change in pyrolysis temperature from 500 to 1500 °C. Electrical conductivity values ranging from 0.100 to 0.385 S cm^{-1} were achieved by the carbon- and metal-based materials used with values comparable to a usual used BES electrode material. The AC conductivity studies revealed hopping conduction mechanism and metal-like conduction due to the incorporation of distinct conductive phases. An acceptable durability in medium conditions over 4 weeks was observed. The biofilm studies revealed adhesion in the first 2 h for most of the surfaces, with a decrease in adhesion and biofilm formation when metal-based materials were introduced. Furthermore, the tailorability of porosity from the micro–meso to meso–macro range and adjustment in hydrophilicity for these materials is also suggested to provide optimized interaction of the biofilm during the BES operation. The flexibility in thickness and sizes, according to the bioreactors sizes, is additionally offered by the tape-casting technique used during the processing of the electrode materials. Finally, this study provides the first findings regarding biofilm on SiOC-based surfaces to be considered in future material development for bioengineering applications.

Compliance with ethical standards

Conflict of interests There are no conflicts to declare.

Data availability The datasets generated during and/or analyzed during the current work are available from the corresponding author on reasonable request.

Electronic supplementary material: The online version of this article (https://doi.org/10.1007/s10853-018-03309-3) contains supplementary material, which is available to authorized users.

References

[1] Conway BE (2013) Electrochemical supercapacitors: scientific fundamentals and technological applications. Springer, New York

[2] Wang G, Zhang L, Zhang J (2012) A review of electrode materials for electrochemical supercapacitors. Chem Soc Rev 41(2):797–828. https://doi.org/10.1039/c1cs15060j

[3] Hwang JY, Myung ST, Sun YK (2017) Sodium-ion batteries: present and future. Chem Soc Rev 46(12):3529–3614. https://doi.org/10.1039/c6cs00776g

[4] Fergus JW (2008) A review of electrolyte and electrode materials for high temperature electrochemical CO_2 and SO_2 gas sensors. Sensor Actuat B-Chem 134(2):1034–1041. https://doi.org/10.1016/j.snb.2008.07.005

[5] Steele BCH, Heinzel A (2001) Materials for fuel-cell technologies. Nature 414(6861):345–352. https://doi.org/10.1038/35104620

[6] Nitta N, Wu FX, Lee JT, Yushin G (2015) Li-ion battery materials: present and future. Mater Today 18(5):252–264. https://doi.org/10.1016/j.mattod.2014.10.040

[7] Zhou MH, Chi ML, Luo JM, He HH, Jin T (2011) An overview of electrode materials in microbial fuel cells. J Power Sources 196(10):4427–4435. https://doi.org/10.1016/j.jpowsour.2011.01.012

[8] Arico AS, Bruce P, Scrosati B, Tarascon JM, Van Schalkwijk W (2005) Nanostructured materials for advanced energy conversion and storage devices. Nat Mater 4(5):366–377. https://doi.org/10.1038/nmat1368

[9] McCreery RL (2008) Advanced carbon electrode materials for molecular electrochemistry. Chem Rev 108(7):2646–2687. https://doi.org/10.1021/cr068076m

[10] Zhang Y, Feng H, Wu XB, Wang LZ, Zhang AQ, Xia TC, Dong HC, Li XF, Zhang LS (2009) Progress of electrochemical capacitor electrode materials: a review. Int J Hydrogen Energy 34(11):4889–4899. https://doi.org/10.1016/j.ijhydene.2009.04.005

[11] Yi Y, Tornow J, Willinger E, Willinger MG, Ranjan C, Schlogl R (2015) Electrochemical degradation of multiwall carbon nanotubes at high anodic potential for oxygen evolution in acidic media. ChemElectroChem 2(12):1929–1937. https://doi.org/10.1002/celc.201500268

[12] Verbrugge MW, Liu P (2005) Microstructural analysis and mathematical modeling of electric double-layer supercapacitors. J Electrochem Soc 152(5):D79–D87. https://doi.org/10.1149/1.1878052

[13] ElMekawy A, Hegab HM, Dominguez-Benetton X, Pant D (2013) Internal resistance of microfluidic microbial fuel cell: challenges and potential opportunities. Bioresour Technol 142:672–682. https://doi.org/10.1016/j.biortech.2013.05.061

[14] Thorne R, Hu HN, Schneider K, Bombelli P, Fisher A, Peter LM, Dent A, Cameron PJ (2011) Porous ceramic anode materials for photo-microbial fuel cells. J Mater Chem 21(44):18055–18060. https://doi.org/10.1039/c1jm13058g

[15] Colombo P, Mera G, Riedel R, Soraru GD (2010) Polymer-derived ceramics: 40 years of research and innovation in advanced ceramics. J Am Ceram Soc 93(7):1805–1837. https://doi.org/10.1111/j.1551-2916.2010.03876.x

[16] Prenzel T, Wilhelm M, Rezwan K (2013) Pyrolyzed polysiloxane membranes with tailorable hydrophobicity, porosity and high specific surface area. Microporous Mesoporous Mat 169:160–167. https://doi.org/10.1016/j.micromeso.2012.10.014

[17] (2013) MAX phases and ultra-high temperature ceramics for extreme environments. In: Low IM, Sakka Y, and Hu CF, (eds). Subscription and registration required for access. Engineering Science Reference, Hershey PA

[18] Harms C, Adam M, Soliman KA, Wilhelm M, Kibler LA, Jacob T, Grathwohl G (2014) New electrocatalysts with pyrolyzed siloxane matrix. Electrocatalysis 5(3):301–309. https://doi.org/10.1007/s12678-014-0190-5

[19] Pradeep VS, Ayana DG, Graczyk-Zajac M, Soraru GD, Riedel R (2015) High rate capability of SiOC ceramic Aerogels with tailored porosity as anode materials for li-ion batteries. Electrochim Acta 157:41–45. https://doi.org/10.1016/j.electacta.2015.01.088

[20] Kolathodi MS, David L, Abass MA, Singh G (2016) Polysiloxane-functionalized graphene oxide paper: pyrolysis and performance as a Li-ion battery and supercapacitor electrode. RSC Adv 6(78):74323–74331. https://doi.org/10.1039/c6ra15746g

[21] Abass MA, Syed AA, Gervais C, Singh G (2017) Synthesis and electrochemical performance of a polymer-derived silicon oxycarbide/boron nitride nanotube composite. RSC Adv 7(35):21576–21584. https://doi.org/10.1039/c7ra01545c

[22] Colombo P, Gambaryan-Roisman T, Scheffler M, Buhler P, Greil P (2001) Conductive ceramic foams from preceramic polymers. J Am Ceram Soc 84(10):2265–2268

[23] Drillet JF, Adam M, Barg S, Herter A, Koch D, Schmidt VM, Wilhelm M (2010) Development of a novel zinc/air fuel cell with a Zn foam anode, a PVA/KOH membrane and a MnO_2/SiOC-based air cathode. ECS Trans 28(32):13–24. https://doi.org/10.1149/1.3506337

[24] Moni P, Wilhelm M, Rezwan K (2017) The influence of carbon nanotubes and graphene oxide sheets on the morphology, porosity, surface characteristics and thermal and electrical properties of polysiloxane derived ceramics. RSC Adv 7(60):37559–37567. https://doi.org/10.1039/c7ra01937h

[25] Scheffler M, Greil P, Berger A, Pippel E, Woltersdorf J (2004) Nickel-catalyzed in situ formation of carbon nanotubes and turbostratic carbon in polymer-derived ceramics. Mater Chem Phys 84(1):131–139. https://doi.org/10.1016/j.matchemphys.2003.11.003

[26] Wu YL, Zhang XL, Li SH, Lv XY, Cheng Y, Wang XM (2013) Microbial biofuel cell operating effectively through carbon nanotube blended with gold-titania nanocomposites modified electrode. Electrochim Acta 109:328–332. https://doi.org/10.1016/j.electacta.2013.07.166

[27] Mehdinia A, Ziaei E, Jabbari A (2014) Facile microwave-assisted synthesized reduced graphene oxide/tin oxide

nanocomposite and using as anode material of microbial fuel cell to improve power generation. Int J Hydrogen Energy 39(20):10724–10730. https://doi.org/10.1016/j.ijhydene.2014.05.008

[28] Varanasi JL, Nayak AK, Sohn Y, Pradhan D, Das D (2016) Improvement of power generation of microbial fuel cell by integrating tungsten oxide electrocatalyst with pure or mixed culture biocatalysts. Electrochim Acta 199:154–163. https://doi.org/10.1016/j.electacta.2016.03.152

[29] Prenzel T, Guedes TLM, Schlüter F, Wilhelm M, Rezwan K (2014) Tailoring surfaces of hybrid ceramics for gas adsorption—from alkanes to CO_2. Sep Purif Technol 129:80–89. https://doi.org/10.1016/j.seppur.2014.03.029

[30] Simões M, Cleto S, Pereira MO, Vieira MJ (2007) Influence of biofilm composition on the resistance to detachment. Water Sci Technol 55(8–9):473–480. https://doi.org/10.2166/wst.2007.293

[31] Lemos M, Gomes I, Mergulhão F, Melo L, Simões M (2015) The effects of surface type on the removal of *Bacillus cereus* and *Pseudomonas fluorescens* single and dual species biofilms. Food Bioprod Process 93:234–241. https://doi.org/10.1016/j.fbp.2014.08.009

[32] Meireles A, Ferreira C, Melo L, Simões M (2017) Comparative stability and efficacy of selected chlorine-based biocides against *Escherichia coli* in planktonic and biofilm states. Food Res Int 102:511–518. https://doi.org/10.1016/j.foodres.2017.09.033

[33] Islam MA, Ethiraj B, Cheng CK, Yousuf A, Khan MMR (2017) Electrogenic and antimethanogenic properties of *Bacillus cereus* for enhanced power generation in anaerobic sludge-driven microbial fuel cells. Energy Fuels 31(6):6132–6139. https://doi.org/10.1021/acs.energyfuels.7b00434

[34] Malheiro J, Gomes I, Borges A, Bastos MMSM, Maillard JY, Borges F, Simões M (2016) Phytochemical profiling as a solution to palliate disinfectant limitations. Biofouling 32(9):1007–1016. https://doi.org/10.1080/08927014.2016.1220550

[35] Wilhelm M, Soltmann C, Koch D, Grathwohl G (2005) Ceramers—functional materials for adsorption techniques. J Eur Ceram Soc 25(2–3):271–276. https://doi.org/10.1016/j.jeurceramsoc.2004.08.008

[36] Adam M, Vakifahmetoglu C, Colombo P, Wilhelm M, Grathwohl G (2014) Polysiloxane—derived ceramics containing nanowires with catalytically active tips. J Am Ceram Soc 97(3):959–966. https://doi.org/10.1111/jace.12708

[37] Colombo P, Abdirashid MO, Guglielmi M, Esposti LMD, Agostini L (1994) Preparation of ceramic composites by active-ftller-controlled-polymer-pyrolysis. MRS Proceedings 346:403. https://doi.org/10.1557/PROC-346-403

[38] Greil P (1998) Near net shape manufacturing of polymer derived ceramics. J Eur Ceram Soc 18(13):1905–1914. https://doi.org/10.1016/S0955-2219(98)00129-0

[39] Lee SW, Jeon BY, Park DH (2010) Effect of bacterial cell size on electricity generation in a single-compartment microbial fuel cell. Biotechnol Lett 32(4):483–487. https://doi.org/10.1007/s10529-009-0184-1

[40] Brunauer S, Deming LS, Deming WE, Teller E (1940) On a theory of the van der Waals adsorption of gases. J Am Chem Soc 62:1723–1732. https://doi.org/10.1021/ja01864a025

[41] IUPAC (1972) Manual of symbols and terminology for physicochemical quantities and units, vol 31. Definitions, Terminology and Symbols in Colloid and Surface Chemistry, Part 1. London Butterworths, Bristol, UK

[42] Colombo P (2008) Engineering porosity in polymer-derived ceramics. J Eur Ceram Soc 28(7):1389–1395. https://doi.org/10.1016/j.jeurceramsoc.2007.12.002

[43] Schmidt H, Koch D, Grathwohl G, Colombo P (2001) Micro-/macroporous ceramics from preceramic precursors. J Am Ceram Soc 84(10):2252–2255

[44] Wilhelm M, Adam M, Bäumer M, Grathwohl G (2008) Synthesis and properties of porous hybrid materials containing metallic nanoparticles. Adv Eng Mater 10(3):241–245. https://doi.org/10.1002/adem.200800019

[45] Duan LQ, Ma QS (2012) Effect of pyrolysis temperature on the pore structure evolution of polysiloxane-derived ceramics. Ceram Int 38(4):2667–2671. https://doi.org/10.1016/j.ceramint.2011.11.033

[46] Brequel H, Parmentier J, Sorar GD, Schiffini L, Enzo S (1999) Study of the phase separation in amorphous silicon oxycarbide glasses under heat treatment. Nanostruct Mater 11(6):721–731. https://doi.org/10.1016/S0965-9773(99)00360-8

[47] Zhang X, Gao J, Hong C, Han J, Han W (2013) Observation of SiC nanodots and nanowires in situ growth in SiOC ceramics. CrystEngComm 15(38):7803–7807. https://doi.org/10.1039/C3CE40924D

[48] Song F, Koo H, Ren D (2015) Effects of material properties on bacterial adhesion and biofilm formation. J Dent Res 94(8):1027–1034. https://doi.org/10.1177/0022034515587690

[49] Zhao ZB, An SS, Xie HJ, Han XL, Wang FH, Jiang Y (2015) The relationship between the hydrophilicity and surface chemical composition microphase separation structure of multicomponent silicone hydrogels. J Phys Chem B 119(30):9780–9786. https://doi.org/10.1021/acs.jpcb.5b04202

[50] Matsuda T, Ito S (1994) Surface coating of hydrophilic-hydrophobic block-copolymers on a poly(acrylonitrile) hemodialyzer reduces platelet-adhesion and its

transmembrane stimulation. Biomaterials 15(6):417–422. https://doi.org/10.1016/0142-9612(94)90219-4

[51] Guo K, Freguia S, Dennis PG, Chen X, Donose BC, Keller J, Gooding JJ, Rabaey K (2013) Effects of surface charge and hydrophobicity on anodic biofilm formation, community composition, and current generation in bioelectrochemical systems. Environ Sci Technol 47(13):7563–7570. https://doi.org/10.1021/es400901u

[52] Santoro C, Guilizzoni M, Correa Baena JP, Pasaogullari U, Casalegno A, Li B, Babanova S, Artyushkova K, Atanassov P (2014) The effects of carbon electrode surface properties on bacteria attachment and start up time of microbial fuel cells. Carbon 67:128–139. https://doi.org/10.1016/j.carbon.2013.09.071

[53] Bajracharya S, ElMekawy A, Srikanth S, Pant D (2015) Cathodes for microbial fuel cells. microbial electrochemical and fuel cells: fundamentals and applications. Woodhead Publishing, Cambridge, pp 179–213

[54] Li A, Han M, Chan SH, N-t Nguyen (2010) Effects of hydrophobicity of the cathode catalyst layer on the performance of a PEM fuel cell. Electrochim Acta 55(8):2706–2711. https://doi.org/10.1016/j.electacta.2009.12.048

[55] Jonscher AK (1977) Universal dielectric response. Nature 267(5613):673–679. https://doi.org/10.1038/267673a0

[56] Cordelair J, Greil P (2000) Electrical conductivity measurements as a microprobe for structure transitions in polysiloxane derived Si–O–C ceramics. J Eur Ceram Soc 20(12):1947–1957. https://doi.org/10.1016/S0955-2219(00)00068-6

[57] Lu K, Erb D, Liu MY (2016) Phase transformation, oxidation stability, and electrical conductivity of TiO_2-polysiloxane derived ceramics. J Mater Sci 51(22):10166–10177. https://doi.org/10.1007/s10853-016-0244-6

[58] Monthioux M, Delverdier O (1996) Thermal behavior of (organosilicon) polymer-derived ceramics. V: main facts and trends. J Eur Ceram Soc 16(7):721–737. https://doi.org/10.1016/0955-2219(95)00186-7

[59] Prabu M, Selvasekarapandian S, Reddy MV, Chowdari BVR (2012) Impedance studies on the 5-V cathode material, $LiCoPO_4$. J Solid State Electrochem 16(5):1833–1839. https://doi.org/10.1007/s10008-012-1670-2

[60] Dyre JC, Schroder TB (2000) Universality of ac conduction in disordered solids. Rev Mod Phys 72(3):873–892. https://doi.org/10.1103/RevModPhys.72.873

[61] Wang XA, Shi ZC, Chen M, Fan RH, Yan KL, Sun K, Pan SB, Yu MX (2014) Tunable electromagnetic properties in Co/Al_2O_3 cermets prepared by wet chemical method. J Am Ceram Soc 97(10):3223–3229. https://doi.org/10.1111/jace.13113

[62] Zhang ZD, Cheng CB, Han X (2016) Percolative cobalt/silicon nitride composites with tunable negative electromagnetic parameters. RSC Adv 6(86):82478–82483. https://doi.org/10.1039/c6ra15529d

[63] Bos R, van der Mei HC, Busscher HJ (1999) Physico-chemistry of initial microbial adhesive interactions–its mechanisms and methods for study. FEMS Microbiol Rev 23(2):179–230

[64] Syed Khadar YA, Balamurugan A, Devarajan VP, Subramanian R, Dinesh Kumar S (2018) Synthesis, characterization and antibacterial activity of cobalt doped cerium oxide (CeO_2:Co) nanoparticles by using hydrothermal method. J Mater Res Technol. https://doi.org/10.1016/j.jmrt.2017.12.005

[65] Vahedi M, Hosseini-Jazani N, Yousefi S, Ghahremani M (2017) Evaluation of anti-bacterial effects of nickel nanoparticles on biofilm production by *Staphylococcus epidermidis*. Iran J Microbiol 9(3):160–168

[66] Sharifahmadian O, Salimijazi HR, Fathi MH, Mostaghimi J, Pershin L (2013) Relationship between surface properties and antibacterial behavior of wire arc spray copper coatings. Surf Coat Tech 233:74–79. https://doi.org/10.1016/j.surfcoat.2013.01.060

[67] Grass G, Rensing C, Solioz M (2011) Metallic copper as an antimicrobial surface. Appl Environ Microbiol 77(5):1541–1547. https://doi.org/10.1128/Aem.02766-10

[68] Baudler A, Schmidt I, Langner M, Greiner A, Schröder U (2015) Does it have to be carbon? Metal anodes in microbial fuel cells and related bioelectrochemical systems. Energ Environ Sci 8(7):2048–2055. https://doi.org/10.1039/C5EE00866B

[69] Zhu X, Logan BE (2014) Copper anode corrosion affects power generation in microbial fuel cells. J Chem Technol Biotechnol 89(3):471–474. https://doi.org/10.1002/jctb.4156